IOP Conf. Series: Journal of Physics: Conf. Series **1249** (2019) 012002 doi:10.1088/1742-6596/1249/1/012002

Characterization of plug and slug multiphase flows by means of image analysis

Manfredo Guilizzoni[1], Giorgio Sotgia[1], Beatrice Baccini, Parham Babakhani Dehkordi, Luigi P. M. Colombo[1]

1) Politecnico di Milano, Department of Energy, Via Lambruschini 4, 20156 Milano, Italy

E-mail: manfredo.guilizzoni@polimi.it

Abstract. Multiphase flow is involved in a wide range of applications, and among the flow patterns that a multiphase mixture may develop in its flow, the intermittent one is particularly complex both in behaviour and for analysis. Experimental analysis about the characteristics of the flow structures (plugs and slugs) is therefore still mandatory for a detailed description of the phenomenon. In this work an image-based technique for the determination of the plug/slug characteristics was applied to air-water, oil-air and three-phase oil-water-air flows in horizontal ducts with different diameters, with superficial velocities of the phases in the range 0.2–2.1 m/s. The technique is based on the acquisition of a video of the flow and the conversion of each frame (or part of it) into a Boolean signal, in which the non-zero part represents the structure of interest. Concatenation of such signals along the singleton dimension creates a space-time representation of the flow, from which information about the flow velocities, the structure lengths and frequencies and the void fraction can be extracted. Focus here is particularly on the performances of the technique when using high-speed videos. The results were also compared with the predictions of the drift-flux model.

1. Introduction

Multiphase flows are involved with great importance in many engineering applications, spanning from energy conversion to chemistry to the oil&gas field. When a multiphase mixture flows within a duct, it exhibits different flow patterns, i.e. different positioning and morphology of the phases in the duct itself, depending on the phases and the velocities. Among the many different possible flow patterns, the intermittent one is characterized by a sequence of plug and slugs, in some cases flowing in pseudo-rigid trains while in other cases chasing one another and coalescing or drifting apart [1]. This flow pattern can be encountered both for two-phase flows during convective boiling and condensation and for three-phase flow in the oil&gas field [2]. In the latter case it may arise from an oil-water flow perturbed by gas bubbles, which is frequent at the exit of an oil well. In all cases the intermittent flow pattern is characterized by a significant complexity both in its behavior and for its analysis, so that experimental investigation about the characteristics of its structures (plugs and slugs) is still mandatory for a detailed description of the phenomenon. A really vast literature is available about the topic and many different techniques and physical principles have been used: intrusive and not intrusive, based on radiation attenuation (in the γ, X, visible, infrared bands), ultrasounds, electric impedance, magnetic resonance; some references to works in this field can be found in [3]. This paper describes the application of an image-based technique for the determination of the plug/slug

Content from this work may be used under the terms of the Creative Commons Attribution 3.0 licence. Any further distribution of this work must maintain attribution to the author(s) and the title of the work, journal citation and DOI.
Published under licence by IOP Publishing Ltd

characteristics to the analysis of air-water, oil-air and three-phase oil-water-air flows. The technique is based on the acquisition of a sequence of flow images, typically from conventional or high-speed videos, but they can also be sequences of radiographies or γ-ray attenuation images. Each frame (or part of it) is first of all converted into a Boolean signal, in which the non-zero part represents the structure of interest. Concatenation of such signals along the singleton dimension creates a space-time representation of the flow, from which information about the structure lengths, frequencies and velocities can be extracted. The latter information is particularly relevant because the cross-section averaged void fraction can also be estimated from the velocities. The technique can be applied to all cases in which a significant difference between the two phases can be observed in the images, i.e. gas-liquid flows and liquid-liquid-gas flows, provided that the latter can be considered as an equivalent gas-liquid flow (e.g. considering oil and water as a single liquid, which is valid within certain ranges of the governing parameters [4]). As examples of the type of images that can be used, some frames from an air-water flow video are included in Fig.1; frames from oil-water-air flows as those investigated in the present work are reported in Fig. 1 of [5]. In fact, the technique was already used with very good results, using videos at 50 fps, for measurement of the velocities in pseudo-stationary intermittent oil-water-air flows [5]. Here the main focus is on the effect of the time resolution on the performance of the technique: therefore, high-speed videos were acquired, in order to process them both at full time resolution and after "subsampling" (see the following section for further details). Superficial velocities of the phases in the range 0.2–2.1 m/s were investigated, for two- and three- phase flow showing the intermittent flow pattern in ducts of different internal diameters (in the range 10–50 mm). The experimental campaign was carried out using the setups available at the Multiphase Fluid Dynamics Laboratory, Department of Energy, Politecnico di Milano (whose description can be found in [6-8]). A Phantom Miro C110 camera with a AF-S Micro NIKKOR 60mm f/2.8G ED lens and a Canon EOS 60D with a EF-S18-135mm lens were used for the high-speed and conventional video respectively. Results were compared also with literature models, finding a very good agreement.

2. Description of the technique

The procedure for the measurement of the bubble/plug/slug parameters consist of the following steps:

- acquisition of a "shadowgraphy" video of the flow, at conventional or high speed, in the visible range or in other spectrum bands (e.g., X- or γ- rays);
- extraction of the single frames and conversion into grayscale if needed;
- selection of a significant (i.e. with large variations of intensity between the phases) set of rows in each frame;
- averaging of the grey intensities along each column of such set to obtain a row vector (where high values represent bubbles);
- concatenation of such signals along the singleton dimension to create a matrix that is a space-time representation of the flow;
- image segmentation to identify the bright stripes (that represent bubbles moving across the observation window, while dark stripes represent the passage of plugs/slugs);
- weighted linear fitting for each bright stripe to determine the slope (in frames/px);
- conversion of the slope into real-world measurement units to obtain the velocity of bubbles in m/s.

Figure 1 reports the described steps with some examples of the intermediate results, together with a summarizing sketch of the procedure and of the obtainable results.

3. Uncertainty and analysis of potential issues

In the technique, many aspects may originate trueness issues:

- hardware: sensor resolution (high enough?), lens optical distortions (negligible?), duct distortions (radial but not axial?), field of view and depth-of-field (optimum?), light (adequate and in proper position/orientation?), time resolution (enough fps?), …

- "software": bit depth (negligible influence?), algorithm and weights for weighted linear regression to determine the slope (optimum?), threshold for identification of the single stripes (significant?), threshold for binarization of the matrix (significant?), …

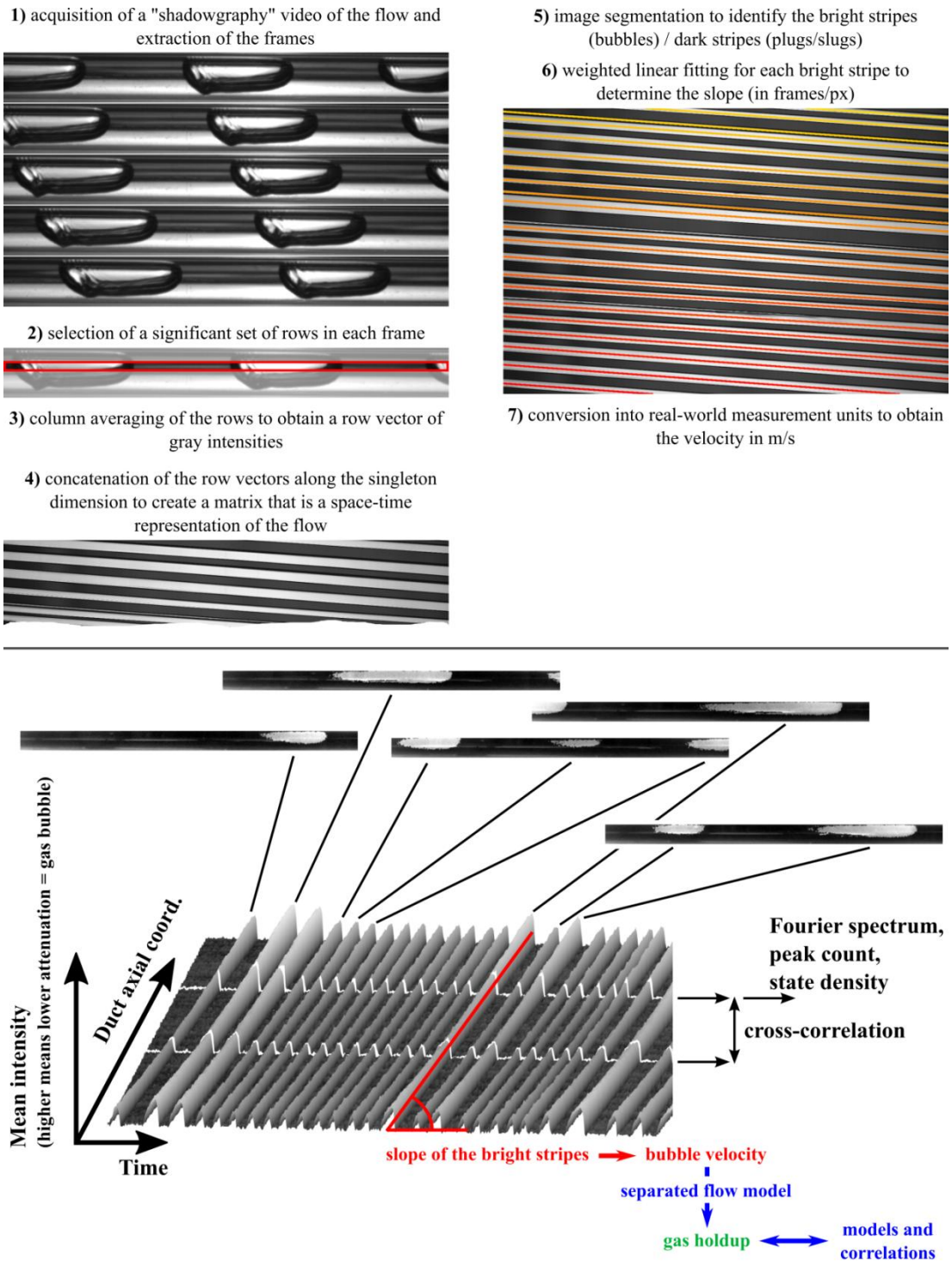

Figure 1. Steps required by the measurement procedure and summarizing sketch of the latter and of the obtainable results.

All of them are very difficult if not impossible to place into a mathematical relationship. In addition, no reference measurement is available. Consequently validation was made *a posteriori* with:

- artificial videos ("cartoons" made by drawings of bubbles or repetitions of single images of real bubbles, in both cases moving at fixed and known velocity). MAPE on the tested cases was 0.27%, with very good accuracy and precision [5]);
- measurements using other techniques and comparison with literature models [5,8,9], in both cases evidencing a very good agreement.

Two aspects that were not thoroughly investigated in the previous work are:

- the influence of the time resolution, which is directly related to the frequency of acquisition of the used videos. The quantity that would be affected most by this is the structure length: when the time resolution is too low, the bands have a thickness of only a few pixels and this greatly reduces the reliability of the measurement (as in this case ±1 px means a large variation). Structure velocity should be less influenced, but in any case it seemed important to perform an in-depth analysis of this potential issue;
- the threshold used for image binarization to identify the single bright/dark stripes.

Thus, high-speed videos were acquired, so that the technique could be applied both using them at full time resolution (using all the original frames) and after sub-sampling (so reducing the number of frames per second). Different binarization threshold were also used.

Air-water flows in a 10 mm i.d. horizontal channel and oil-water-air flows in a 50 mm i.d. horizontal channel were investigated. For the first, superficial velocities in the range J_w = 0.09–0.20 m/s for water and J_a 0.20–1.22 m/s for air were investigated; for the second, a single flow pattern (characterized by superficial velocities J_o = 0.22 m/s for oil, J_w = 0.85 m/s for water and J_a = 0.98 m/s for air) was repeated thrice, to assess repeatability too.

The results evidenced that the influence of both the threshold and the time resolution is very small for the large majority of the flow structures and only for a small number of them it exceeds 2–3%. In terms of the average velocity, the variation over the whole range of investigated thresholds and time resolutions is lower than 1.5%. Figure 2 shows the matrices resulting from the application of the proposed procedure to an air-water flow in a 10 mm i.d. duct, with J_w = 0.09 m/s and J_a = 0.20 m/s, at different time resolutions. As each acquired frame originates a row in the resulting matrix, the original matrices were all of different height; while their width is the same for all, as it corresponds to the width of the acquired frames. For visualization purposes they were then scaled to give them the same height, while conserving the aspect ratio.

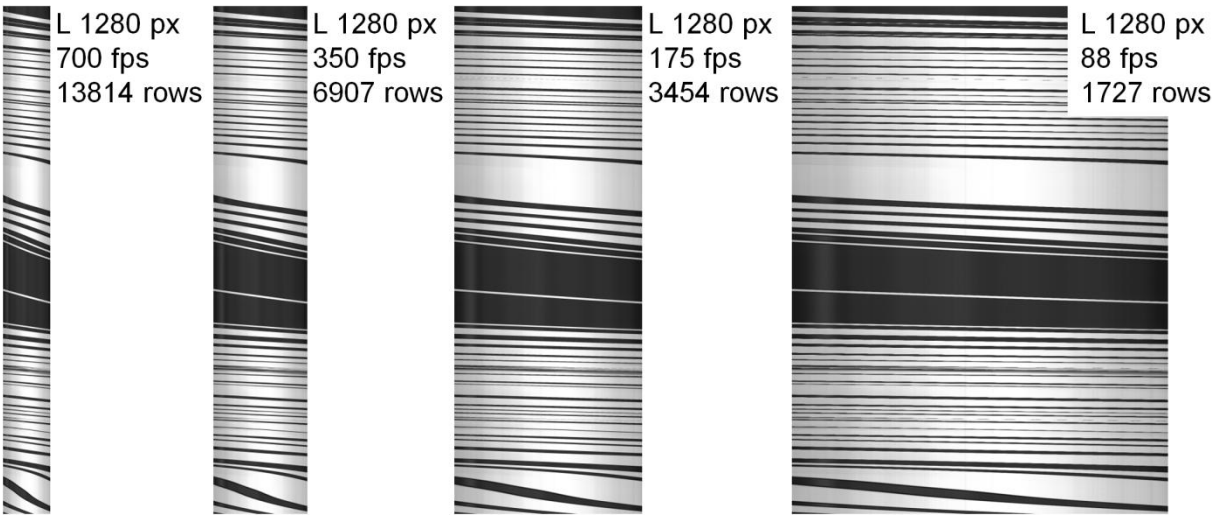

Figure 2. Matrices resulting from the application of the proposed procedure to an air-water flow in a 10 mm i.d. duct, with J_w = 0.09 m/s, J_a = 0.20 m/s, at different time resolutions.

It is evident how the passage of the flow structures is memorized in the matrix: thin bright stripes represent short bubbles, while large ones, long bubbles. Large dark stripes correspond to periods with water filling the duct. It was evident at visual observation that the first bubbles passing during the sampling interval were moving relatively slowly, than some bubbles passed with higher velocities, afterwards a second reduction in the velocity and a final new increase happened. This is perfectly evident in the matrices, where the stripes have different slopes. It can also be noticed how many bubbles changed their velocity (and in some cases also their length) within the "observation window", i.e. the observed part of the duct: the slope and the width of the stripes are not constant.

Figures 3 and 4 report the measured velocities for the bubbles in this investigated flow condition, when varying the time resolution and the threshold for identification of the stripes. The bubble velocities are smoothly varying between a bubble and the following, with an overall oscillating behavior. This was confirmed also for the other investigated air-water flow patterns (compare Fig. 14) and it seems likely to be an effect of the air injection system on the setup used for air-water flows.

Figure 5 shows the matrices resulting from the application of the proposed procedure for an oil-water-air flow in a 50 mm i.d. duct, with J_o = 0.22 m/s, J_w = 0.85 m/s, J_a = 0.98 m/s, at different time resolutions. As before, the matrices were scaled to have the same height for visualization purposes. The lines fitting each bright stripes are also superposed to all the matrices, even if due to the scaling they are visible only in the last image on the right. It can be noticed how in this case the lines are still of different width, but much more regular in slope, meaning that the structure velocities are very similar. This is confirmed by the values of the measured velocities, reported in Fig. 6 for different time resolutions. There are some cases in which the difference between the measured velocities for the single bubbles is significant (up to 10%) when considering the extreme time resolutions (e.g. 31 vs 1000 fps), while it is negligible for the vast majority of the cases when comparing the intermediate resolutions.

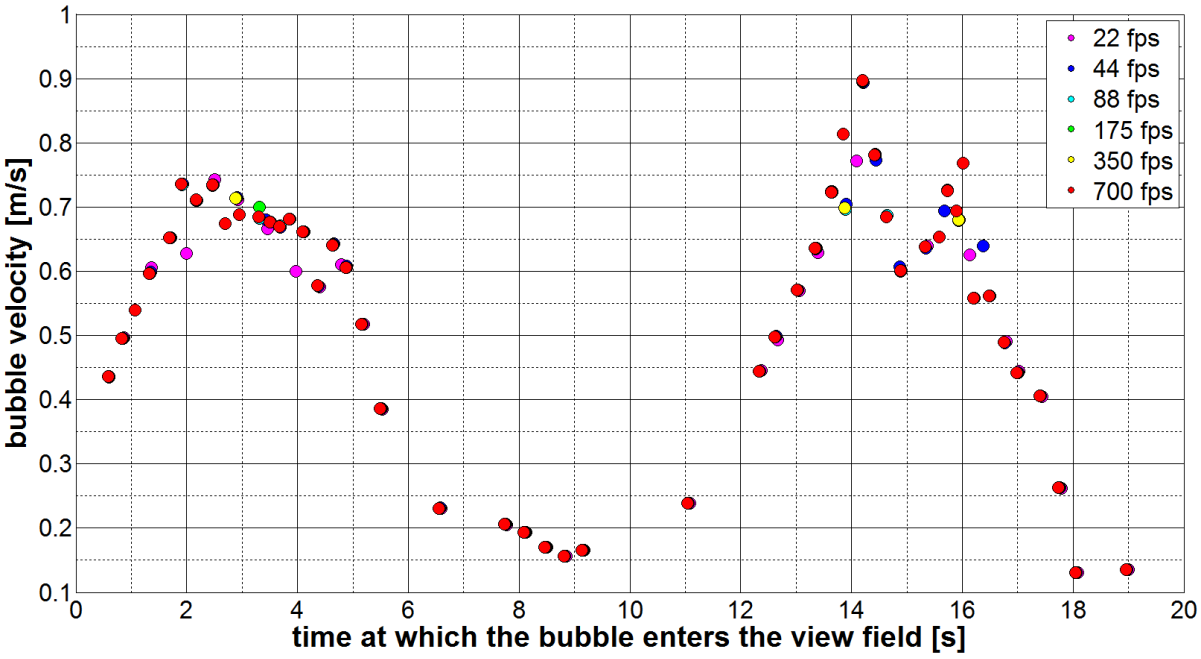

Figure 3. Measured bubble velocities for the J_w = 0.09 m/s, J_a = 0.20 m/s air-water flow in a 10 mm i.d. duct, at different time resolutions.

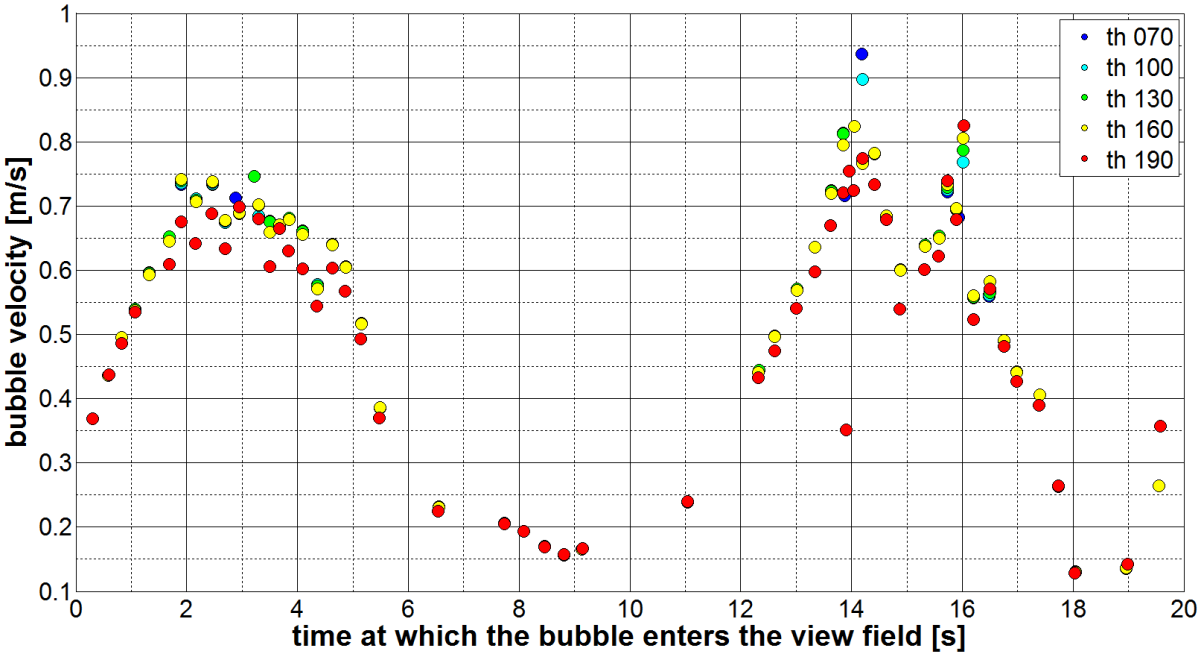

Figure 4. Measured bubble velocities for the J_w = 0.09 m/s, J_a = 0.20 m/s air-water flow in a 10 mm i.d. duct, for different values of the threshold for stripe identification.

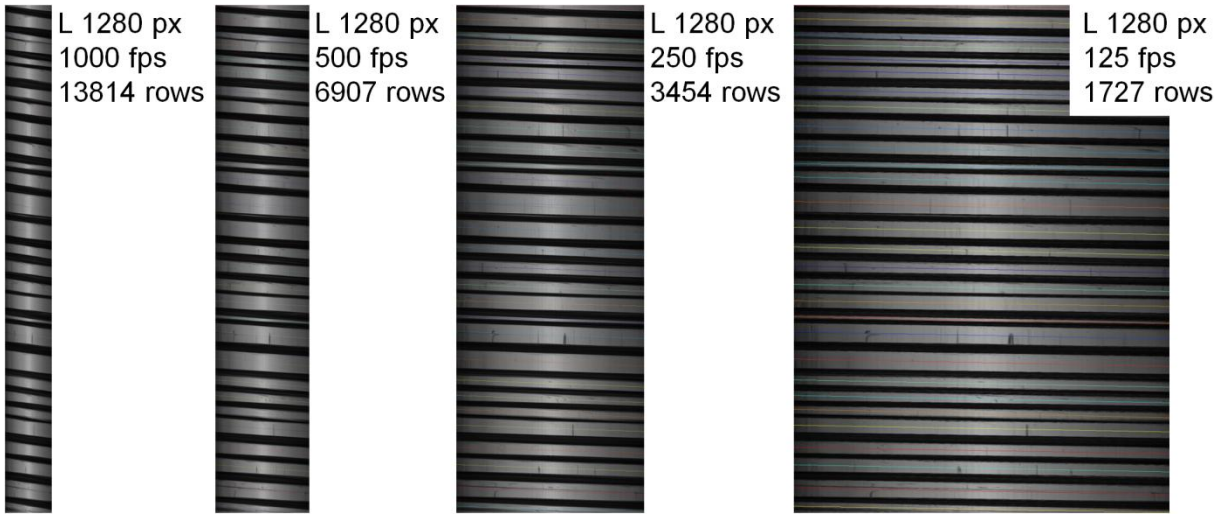

Figure 5. Matrices resulting from the application of the proposed procedure for an oil-air-water flow in a 50 mm i.d. duct, with J_o = 0.22 m/s, J_w = 0.85 m/s, J_a = 0.98 m/s, at different time resolutions. The lines fitting each bright stripes are also superposed to all the matrices, even if due to the scaling they are visible only in the last image on the right.

The median velocity for the bubbles is also reported in Fig. 6 for the different time resolutions: for this quantity the difference is absolutely negligible (in fact the values are identical up to 0.1 m/s accuracy). The fact that in this flow pattern the bubbles move practically at the same velocity was also confirmed by direct observation of the flow, in which bubbles appear to move as a rigid train, never reaching each other.

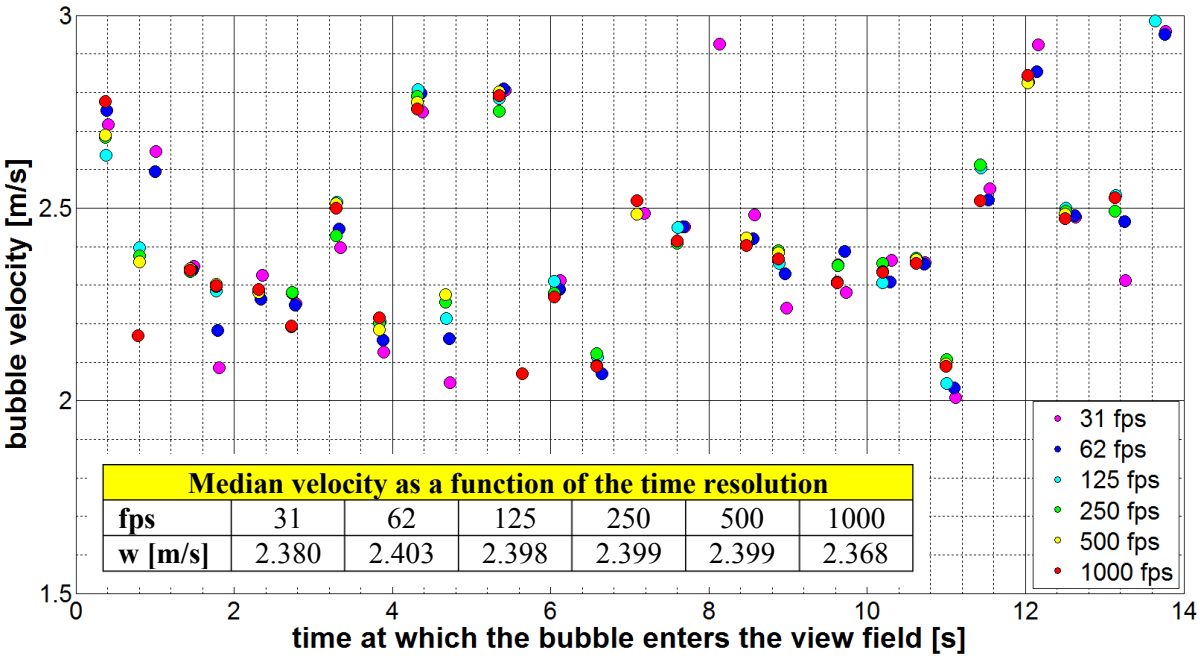

Median velocity as a function of the time resolution						
fps	31	62	125	250	500	1000
w [m/s]	2.380	2.403	2.398	2.399	2.399	2.368

Figure 6. Measured bubble velocities for the J_w = 0.09 m/s, J_a = 0.20 m/s oil-water-air flow in a 50 mm i.d. duct, at different time resolutions. Median bubble velocity w calculated at each time resolution is also reported.

4. Results

After the analysis of the influence of the time resolution and the threshold, the technique was applied to measure bubble velocity, frequency and length for different two- and three-phase flows (for the latter under the assumption of "equivalent liquid" for oil and water) in horizontal ducts:

- 3 air-oil flows in a 50 mm i.d. duct, by conventional speed videos;
- 6 air-water flows in a 10 mm i.d. duct, by high-speed videos;
- 3 oil-water-air flows in a 50 mm i.d. duct, by high-speed videos;
- 90 oil-water-air-oil flows in a 50 mm i.d. duct, by conventional speed videos (for the latter results in terms of bubble velocities were already presented in [5]).

Superficial velocities cover the ranges 0.48–0.72 m/s for oil, 0.09–1.33 m/s for water, 0.20–2.11 m/s for air.

Figure 7 reports the results for all the above cited flow conditions, in terms of bubble velocities as a function of the ratio ε_{gl} between the gas superficial velocity and the total liquid superficial velocity (for three-phase flows the sum of the oil and water superficial velocities). From the measured bubble velocity, the cross-section averaged gas *in situ* gas volume fraction (void fraction) H_g can be estimated (as $H_g = J_g / w_g$). Results can be then compared with the predictions of models and correlations. Figure 8 shows a parity plot referring to the comparison with the drift-flux model [10] (with parameter C_0 = 1.2). Very good agreement is found for the pseudo-stationary flow patterns, while disagreement is evident for the air-water flows, in which bubble velocities were continuously varying (thus giving a not fully developed flow condition).

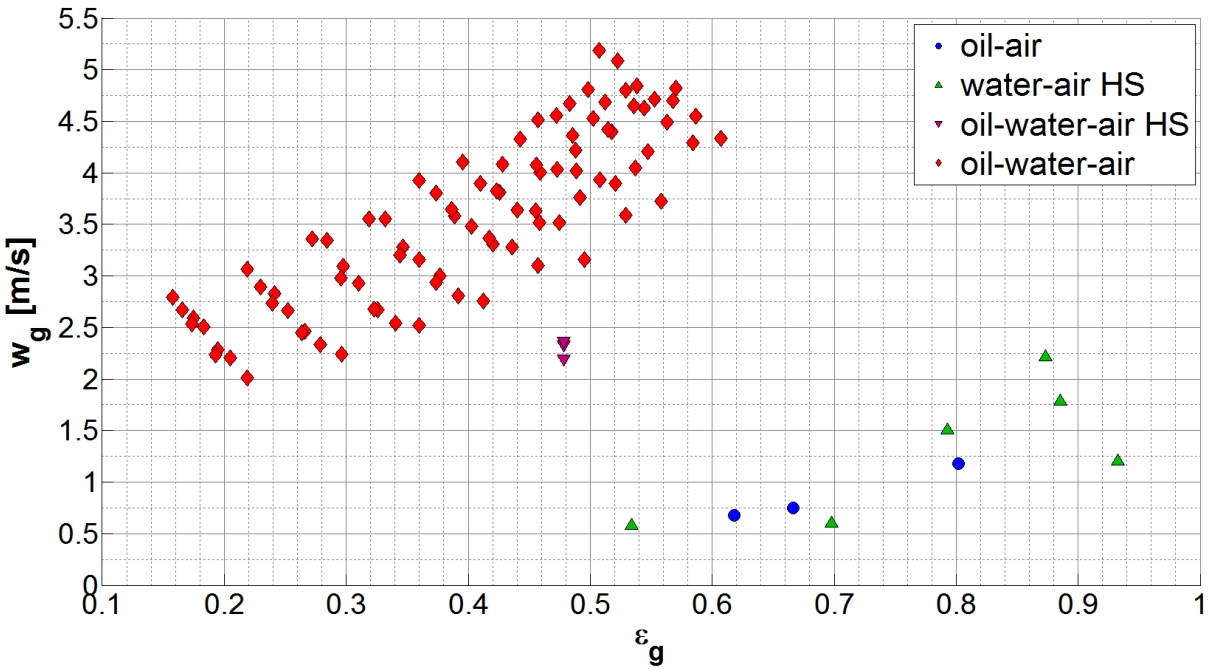

Figure 7. Velocity of the gas bubbles measured with the proposed technique for all the investigated flow conditions, as a function of ε_{gl}.

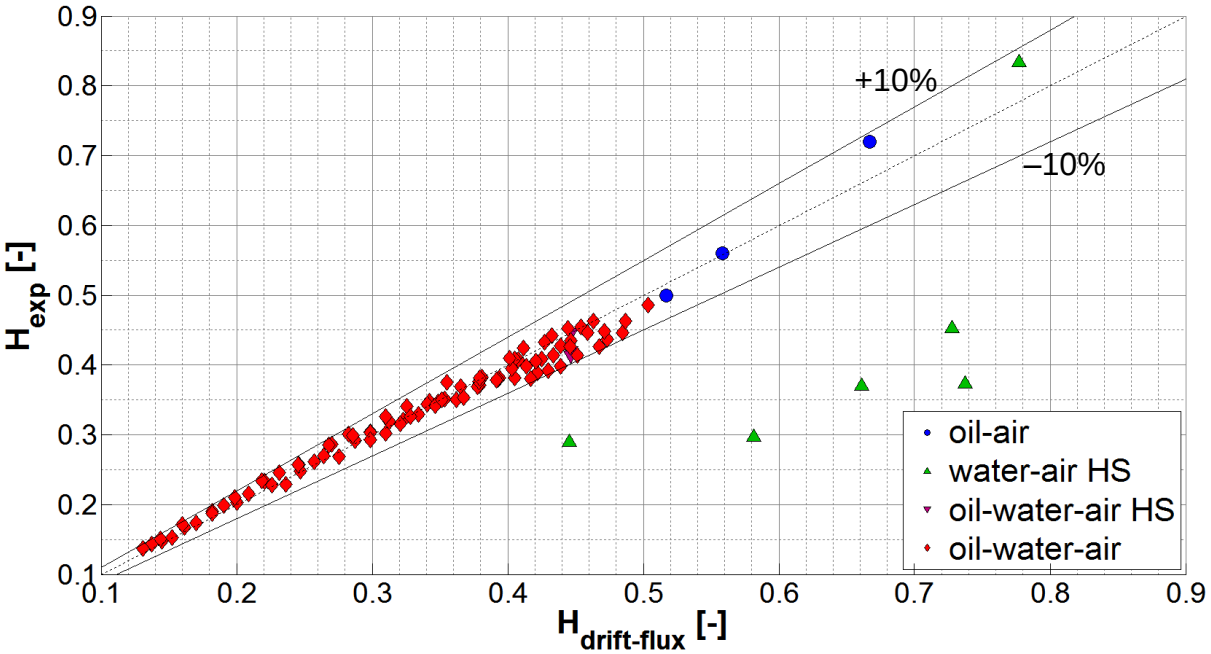

Figure 8. Parity plot of the experimental *in situ* gas volume fraction estimated with the proposed technique compared with the predictions of the drift flux model with $C_0 = 1.2$, for all the investigated flow conditions.

In terms of bubble lengths, Fig. 9 shows the bubble lengths measured for all the investigated three-phase flows, again as a function of ε_{gl}. The "error bars" represent ± the standard deviation for each flow condition. As already said, a minor amount of the latter can be ascribed at the measurement

uncertainty (the majority of the data were acquired at conventional video speed), but the major contribution is the intrinsic variation in the physical flow pattern. It can be noticed how both the bubble length and its variability largely increase at increasing ε_{gl}.

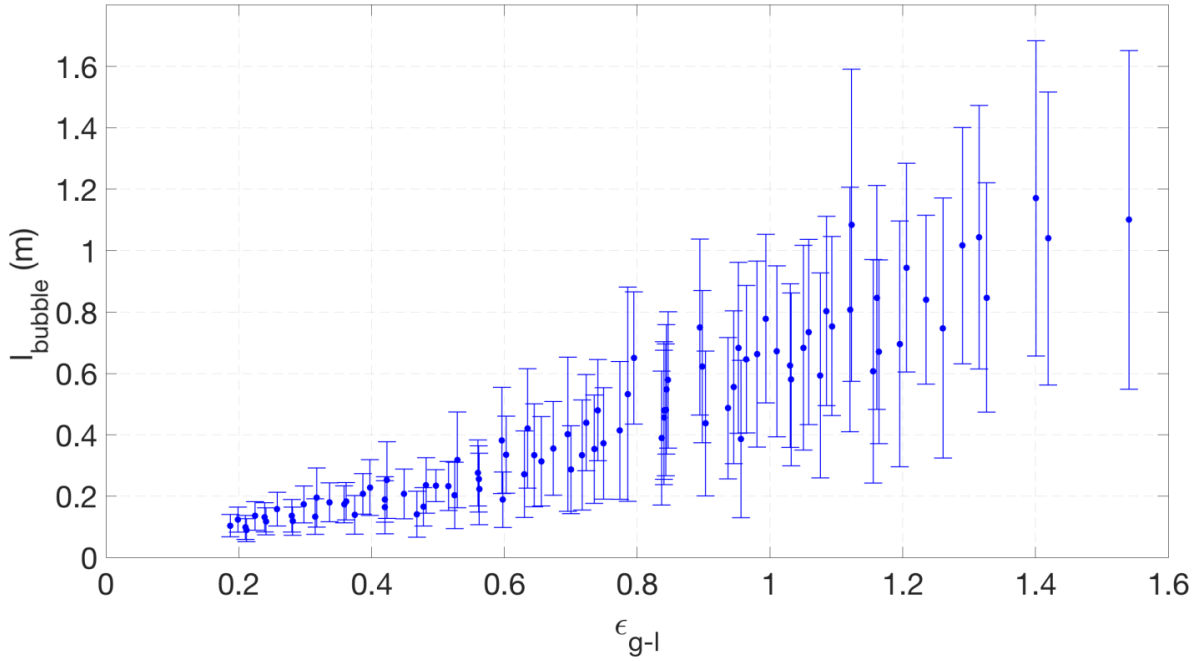

Figure 9. Length of the gas bubbles measured with the proposed technique for all the investigated three-phase flow conditions, as a function of ε_{gl}.

To further evidence the separate effect of the oil and water velocities on the bubble length variability, Fig. 10 shows the latter as a function of the bubble length, with marker colors proportional to J_o (panel a) and J_w (panel b).

Finally, Figs. 11 and 12 report the resulting matrix, the sequence of bubble velocities and the power spectrum calculated from three columns of the matrix, for an air-water flow in a 10 mm i.d., with J_w = 0.18 m/s, J_a = 0.20 m/s. It can be observed how also in this case the bubble velocities are smoothly oscillating within the sampling interval. As it can be seen from Fig. 13, for this case the agreement between the bubble frequency predicted by the Fourier transform of the columns on the matrix and the value obtained by simple bubble count in the sampling interval is good, even if significantly dependent on the threshold chosen for bubble count. For other cases the discrepancy between the two values becomes larger, even if typically confined within 15%. In any case, bubble count appears to be a simpler and more reliable method to determine the bubble frequency, particularly for cases in which a small number of bubbles cross the observation window during the sampling interval. In fact, for such cases the Fourier spectrum is calculated on a short square-wave function, which is problematic for Fourier transform.

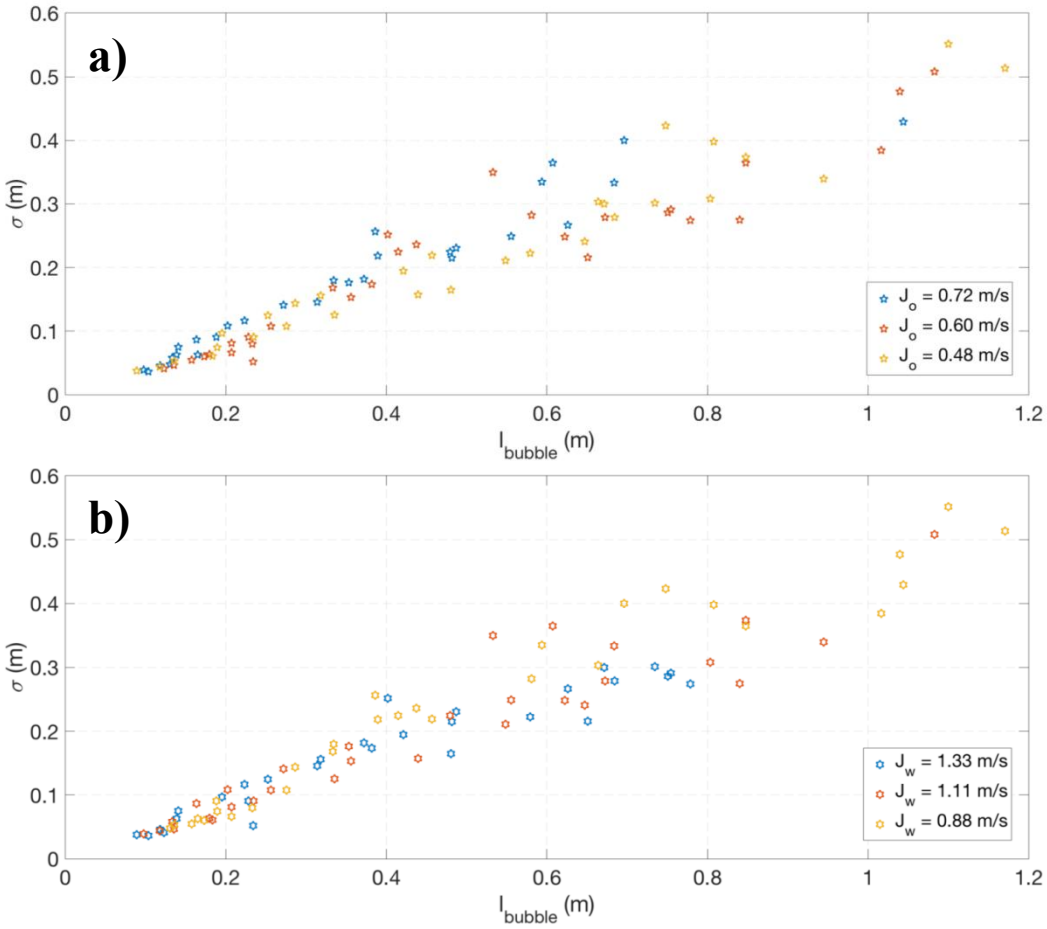

Figure 10. Standard deviation of gas bubble lengths measured with the proposed technique for all the investigated three-phase flow conditions, as a function of the bubble length. Marker colors are proportional to J_o in panel a) and to J_w in panel b).

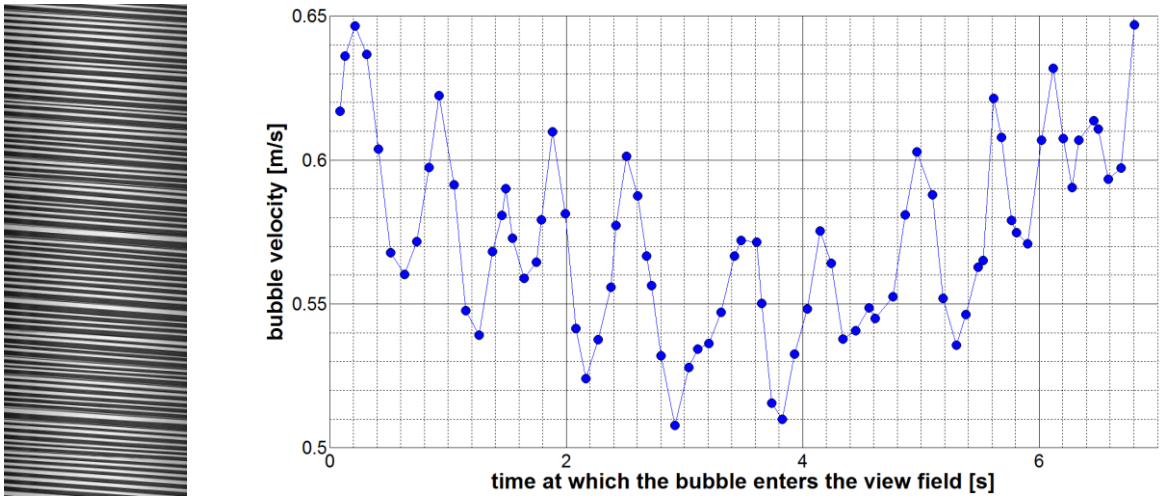

Figure 11. The matrix calculated with the proposed procedure and the measured bubble velocities for an air-water flow in a 10 mm i.d., with J_w = 0.18 m/s, J_a = 0.20 m/s.

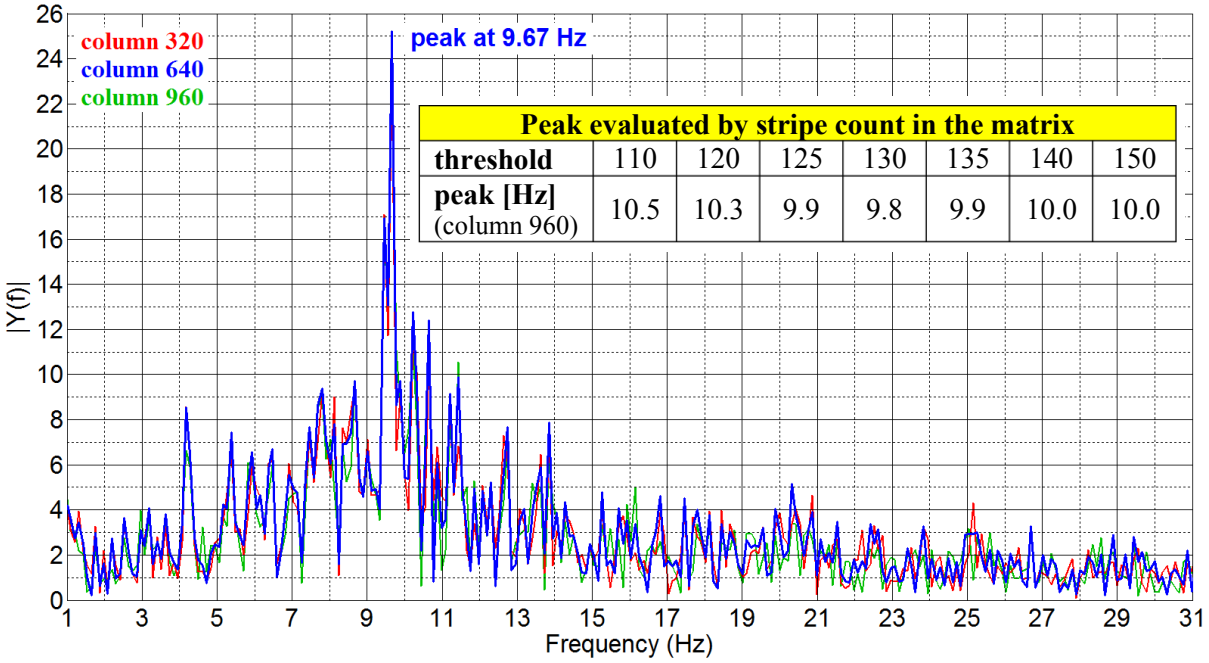

Figure 12. Power spectrum for an air-water flow in a 10 mm i.d., with J_w = 0.18 m/s, J_a = 0.20 m/s. Bubble frequency calculated using the proposed procedure, for different values of the threshold for stripe identification, is also reported in the inset table.

5. Conclusions

A technique, based on image processing of videos at conventional or high speed, was developed to measure the structure velocities, lengths and frequencies for two-phase and three-phase flows. It was tested on air-water, oil-air and oil-water-air flows, with particular focus on the sensitivity of the technique with respect to the time resolution of the videos and the threshold used for identification of the flow structures. A negligible effect of both was confirmed in the measurement of the velocities, while a more significant influence was observed for the bubble lengths and frequencies – in any case with variations that are well within the usual uncertainty ranges for measurements on multiphase flows. The measured velocities were also used to estimate the cross-section averaged void fraction, that was then compared with the predictions of the drift-flux model, evidencing a very good agreement for developed pseudo-stationary flows. The technique proved also effective in quantifying the periodic oscillations in the structure velocities that characterize some flow conditions.

Nomenclature

C_0	distribution parameter in the drift-flux model (-)
H	*in situ* volume fraction (void fraction) (-)
J	superficial velocity (m/s)
L	width of the frames (px)
MAPE	mean absolute percentage error (%)
w	actual velocity (m/s)

Greek Symbols

ε	volume ratio (-)

Subscripts and superscripts

a	air
g	gas
l	liquid
o	oil
w	water

References

[1] Fabre J and Liné A 2019. Slug flow (available online at: http://www.thermopedia.com/content/38, accessed March 2019), https://doi.org/10.1615/AtoZ.s.slug_flow

[2] Hall A 2019 Three-phase, gas-liquid-liquid flows (available online at: http://www. thermopedia.com/content/270 , accessed november 2019), https://doi.org/10.1615/AtoZ.t.three_phase_gas-liquid-liquid_flows

[3] Guilizzoni M 2013 Flow pattern identification in gas–liquid flows by means of phase density imaging *Int J Multiph Flow* 5**1** 1–10, https://doi.org/10.1016/j.ijmultiphaseflow.2012.11.006

[4] Poesio P, Sotgia G, Strazza D 2009 Experimental investigation of three-phase oil-water-air flow through a pipeline *Multiph. Sci. Technol.* **21** (1–2) 107–22, https://doi.org/10.1615/MultScienTechn.v21.i1-2.90

[5] Guilizzoni M, Baccini B, Sotgia G, Colombo L P M 2018 Image-based analysis of intermittent three-phase flow *Int J Multiph Flow* **107** 256–62, https://doi.org/10.1016/j.ijmultiphaseflow.2018.06.019

[6] Colombo L P M, Guilizzoni M, Sotgia G 2012 Characterization of the critical transition from annular to wavy-stratified flow for oil-water mixtures in horizontal pipes *Exp. Fluids* **53**(5) 1617–25, https://doi.org/10.1007/s00348-012-1378-1

[7] Babakhani Dehkordi P., Colombo L P M, Colombo, Guilizzoni M, Sotgia G, Cozzi F 2017 Quantitative visualization of oil-water mixture behind sudden expansion by high speed camera 2017 *J. Phys.: Conf. Ser.* **882** 012009, https://doi.org/10.1088/1742-6596/882/1/012009

[8] Baccini B 2016 Experimental characterization of pressure gradients and flow structure for viscous oil-water-air flows in horizontal pipes, M.Sc. thesis, advisor prof. M. Guilizzoni, Politecnico di Milano, https://www.politesi.polimi.it/handle/10589/129161

[9] Babakhani Dehkordi P 2017 Experimental and numerical analysis of multiphase flow within horizontal pipeline with variable cross-sectional area. Energy and Nuclear Science and Technology, Ph.D. dissertation, advisor prof. L. Colombo, Politecnico di Milano, http://hdl.handle.net/10589/136203

[10] Zuber N, Findlay J A 1965 Average volumetric concentration in two-phase flow systems *J. Heat Transf.* **87** (4) 453–68, https://doi.org/10.1115/1.3689137